[Journal Name

ARTICLE TYPE

Cite this: DOI: 00.0000/xxxxxxxxxx

Supplemental information

Elia Missi,[a] Agnès Montillet,[b] Isabelle Capron,[c], Jérôme Bellettre,[a] and Teodor Burghelea[a†]

Received Date
Accepted Date

DOI: 00.0000/xxxxxxxxxx

A Size exclusion chromatography measurements

The molar mass of the xanthan gum used through this study was measured by means of size-exclusion chromatography (*SEC*), combined with light scattering, viscometer and concentration detectors (known as triple detection), using the *OMNISEC*$*$ apparatus from Malvern Panalytical. Light scattering detectors measure the intensity of the light scattered by the sample which directly relates to the molar mass and can also be used to calculate the radius of gyration (Rg) of the molecules. The repeatability of the *SEC* measurements has been carefully checked by repeating the tests several times.

We illustrate in Fig. 1 a graphical output of an *SEC* measurement performed with a $C_{XG} = 1\%$ xanthan solution.

A comparative summary of the results of *SEC* measurements performed for two xanthan concentrations chosen within the gel-like regime is compiled in Tab. 1.

B Macro-rheological measurements

The parallel plate rheological setup is schematically illustrated in Fig. 2.

To prevent the emergence of wall slip that is known to induce measurement artifacts[1,2] we have used a sandblasted top disk **D** with a radius $R = 17.5\ mm$. The glass-made bottom plate **PP** was equally serrated and its temperature was controlled via Peltier plate. By performing steady state viscosity measurements for various values of the gap, we have ruled out the emergence of the wall slip. For the experiments reported through the paper, the gap between the plates was $d = 1\ mm$.

Two distinct rotational rheological protocols have been used for the characterization of the xanthan solutions.

First, linearly increasing/decreasing controlled stress ramps as schematically illustrated in Fig. 2(b) have been performed. The maximum applied stress τ_{max} has been judiciously chosen for each concentration of xanthan in order to cover a range of deformation states as wide as possible while avoiding the emergence of inertial instabilities which are known to bias the rheological tests,[1,3]. Both the increasing stress and decreasing stress branch of the linear stress ramp consisted of $N = 750$ steps. The waiting time per stress value t_0 to be further referred to as the characteristic time of the external forcing was varied from $t_0 = 0.2\ s$ to $t_0 = 5\ s$. Corresponding to the largest value of the waiting

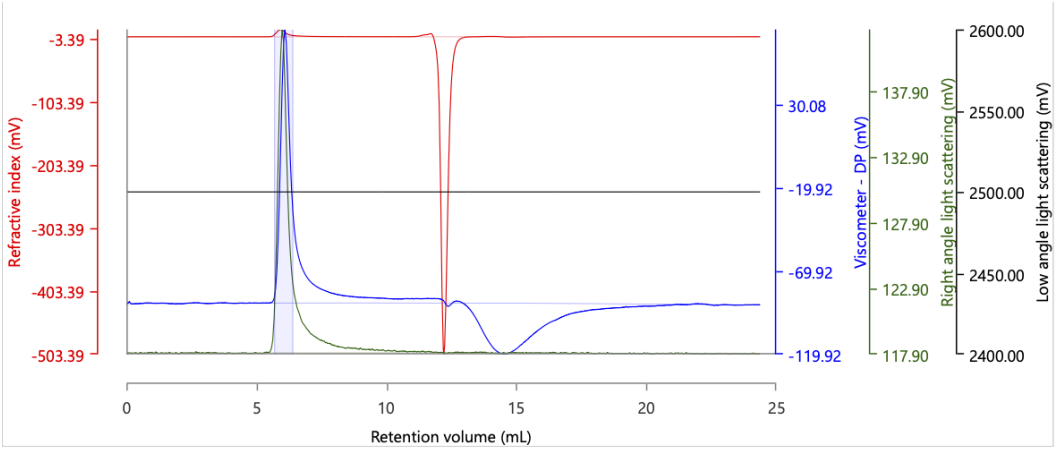

Results

	X 1%-0-NaCl Injection 1 Peak 1 15/6/23 11:01:11
RV (mL)	5.93
Mn (g/mol)	1 302 406
Mw (g/mol)	1 330 434
Mz (g/mol)	1 353 972
Mw/Mn	1.022
Mp (g/mol)	1 460 632
IVw (dL/g)	17.1659
Rh(η)w (nm)	71.05
Rgw (nm)	83.8
M-H a	N/C
M-H log K (dL/g)	N/C
Frac. of sample (%)	100
Measured conc. (mg/mL)	0.0764
Recovery (%)	38.21
Calc. dn/dc (mL/g)	N/C
RI peak (mV·mL)	4.7
RALS peak (mV·mL)	10.13
LALS peak (mV·mL)	1 750
DP peak (mV·mL)	67.58

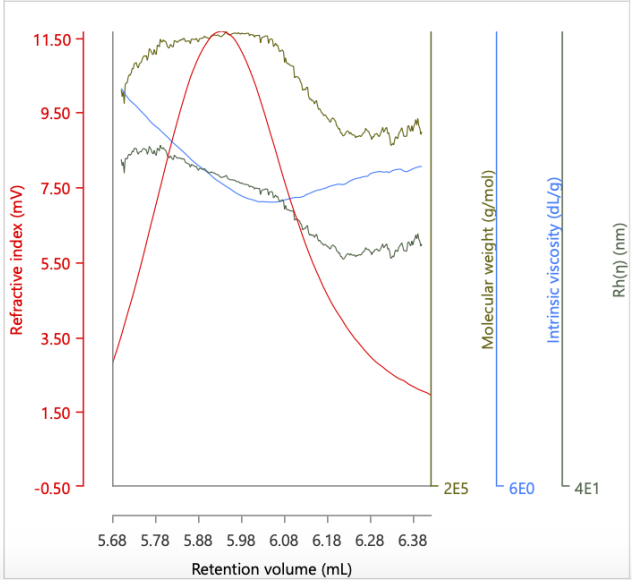

Fig. 1 Example of SEC measurement results with $C_{XG} = 1\%$.

	$\mathbf{C_{XG} = 0.5\%}$	$\mathbf{C_{XG} = 0.5\%}$ **0.1M NaCl**	$\mathbf{C_{XG} = 1\%}$	$\mathbf{C_{XG} = 1\%}$ **0.1M NaCl**
$\mathbf{RV(mL)}$	6.06	5.97	5.96	5.95
$\mathbf{M_n(g/mol)}$	1348786	1478448	1162781	1559365
$\mathbf{M_w(g/mol)}$	1354594	1490476	1194244	1575171
$\mathbf{M_z(g/mol)}$	1360082	1502012	1222260	1589950
$\mathbf{M_w/M_n}$	1.004	1.008	1.027	1.01
$\mathbf{IVw(dL/g)}$	18.1194	17.8546	17.0693	17.8574
$\mathbf{Rhw(nm)}$	72.96	74.94	68.29	76.2
$\mathbf{Rgw(nm)}$	83.81	85.3	82.21	83.47
$\mathbf{M-H\ a}$	N/C	N/C	-0.849	N/C
$\mathbf{M-H\ logK\ (dL/g)}$	N/C	N/C	6.425	N/C
Measured conc. $\mathbf{(mg/mL)}$	0.1534	0.1461	0.0645	0.0296
$\mathbf{Recovery(\%)}$	30 .68	29.21	32.25	14.8
RI peak $\mathbf{(mV \cdot mL)}$	9.79	9.31	3.98	1.82
RALS peak $\mathbf{(mV \cdot mL)}$	21.37	21.7	8.07	4.61
LALS peak $\mathbf{(mV \cdot mL)}$	1749.42	1759.08	1760.62	1709.69
DP peak $\mathbf{(mV \cdot mL)}$	144.59	135.37	56.81	27.13
MALS peak $\mathbf{(mV \cdot mL)}$	1.33	1.32	0.49	0.29

Table 1 Summary of SEC measurements performed with $C_{XG} = 0.5\%$ and $C_{XG} = 1\%$ xanthan solutions.

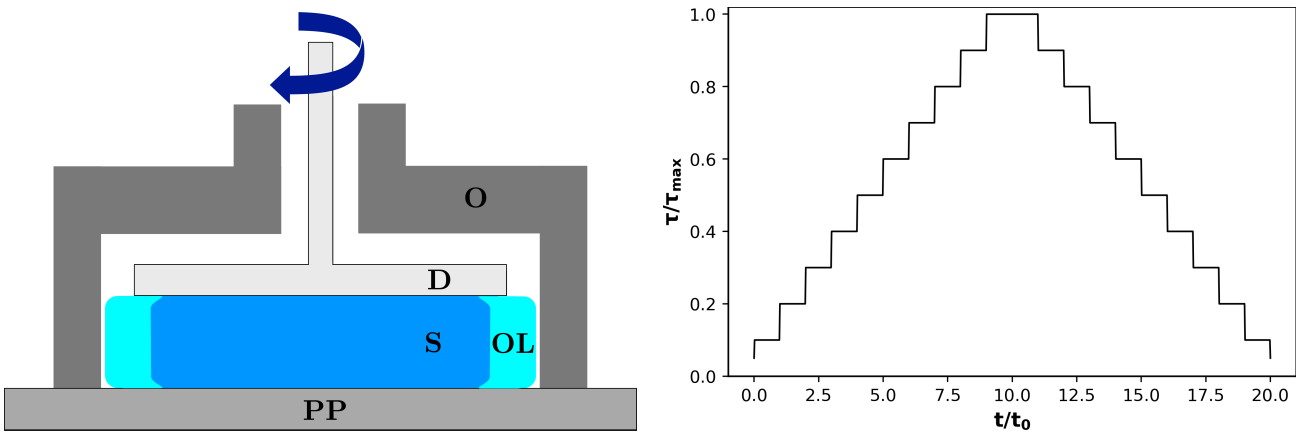

(a) (b)

Fig. 2 (a)Schematic representation of the rheometric setup: D - top rotating disk, PP bottom Peltier plate, S - sample, OL - protective oil layer, O - electric oven. (b) Schematic representation of the linear stepped stress ramp. The time per stress step is t_0. For clarity of the presentation, we have chosen here $N = 10$ steps of each of the two branches of the ramp while during the experiments we report herein $N = 750$.

time, steady state measurements of the viscosity were performed. We have verified using a $5mPas$ standard calibration oil that accuracy of the viscosity measurements within a range of small applied stresses ($\tau \in [0.05Pa - 0.5Pa]$) is about 0.5%. This ensures the reliability of the zero shear viscosity measurements for all xanthan concentrations explored.

The results of the controlled stress ramps are presented in terms of the dependence of the absolute value of the rate of deformation on the applied stress. We note that the choice of the representation $(\tau - |\dot{\gamma}|)$ for displaying the results is less popular within the rheological community and a brief motivation for its choice here is in order. In the context of the upcoming discussion, the choice of this representation has several clear advantages against the more widely used representations $(\dot{\gamma} - \eta)$ or $(\tau - \eta)$ as follows. First and from a qualitative standpoint, plotting the rates of the deformation on the vertical axis allows one to better identify the viscoplastic rheological behavior by associating flow states characterized by $|\dot{\gamma}| \ll 1s^{-1}$ to solid deformation states and the rest by fluid ones. From a more quantitative standpoint, recall that the increasing/decreasing stress ramps are linear in time (see Fig. 2(b)), flow states characterized by $|\dot{\gamma}| \approx$ ct. correspond to strains that are proportional to the applied stress $\gamma \propto \tau$ which is a clear signature of a Hookean elastic solid behavior. Last, monitoring the absolute values of the rates of the deformation $|\dot{\gamma}|$ rather than the rates of the deformation $\dot{\gamma}$ allows to accurately pinpoint in a log-log scale flow reversal during the flow curves where the rates of deformation change sign.

A second rheometric protocol employed through this study was the creep test. Such tests were performed by imposing a constant stress σ_0 and monitoring the time evolution of the deformation γ. In the asymptotic limit of large time, a linear time dependence of the strain is understood as a signature of fluid rheological behavior while a sub-linear one is interpreted as a signature of solid rheological behavior,[2,4]. The creep tests reported herein were solely performed at an ambient temperature, $T = 298\ K$.

As thermo-rheological analysis plays an important role through this study, a particular attention has been paid to the thermal regulation during the rheological tests. The temperature was regulated

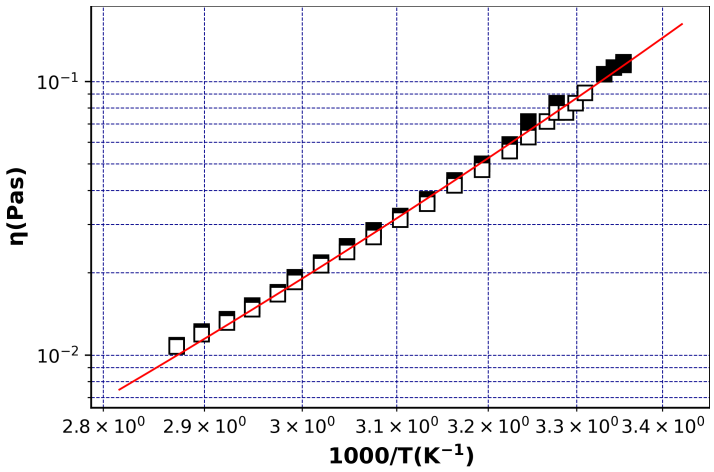

Fig. 3 Viscosity measurements performed with a Newtonian oil during a linear ramp in temperature between $T_{min} = 298\ K$, $T_{max} = 348\ K$. The full/empty symbols refer to increasing/decreasing branch of the ramp. The full line is a nonlinear fitting function according to the Arrhenius law.

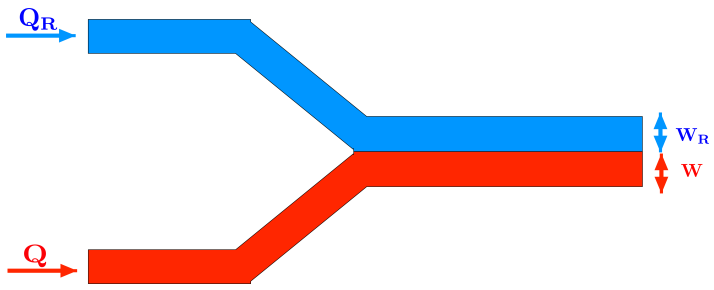

Fig. 4 Schematic representation of the high shear rate microfluidic rheometer: Q - flow rate of the fluid to be characterized, Q_R - flow rate of the reference fluid with a known viscosity, W - transversal extent of the fluid to be characterized, W_R - transversal extent of the fluid reference fluid.

at values ranging in between 25 ± 0.05^oC and 75 ± 0.05^oC using both the Peltier system embedded in the bottom plate **PP** of the rheometer and an electrical oven enclosure **O** mounted on the top of the geometry, Fig. 2(a). The viscosity data acquired during temperature ramps were corrected using the *"Thermo gap*" option of the rheometer which accounts for the thermal expansion of the solid parts of the rheometric geometry. To prevent the evaporation of the fluid sample **S** which may become critically important during long rheometric tests performed at temperatures larger than the ambient temperature, the free meniscus of the solution has been covered with a thin layer of oil **OL**, Fig. 2(a). As compared to the viscosities of the tested xanthan solutions, the viscosity of the oil was significantly smaller, $\eta_0 = 5mPas$.

C High shear rate microfluidic rheometry

To measure the shear viscosity in a high range of rates of shear that are not accessible via classical rotational rheometry techniques, we have used a microfluidic rheometric system, Fig. 4. A detailed description of the operating principle of this device can be found in[5]. The fluid to be characterized is injected side by side (co flowing) with a reference fluid (with a known viscosity) in Y shaped

micro-channel[6] with a width $W_{total} = W + W_R = 2200\ \mu m$ as schematically illustrated in Fig. 4. Using successively two microchips with channels of different heights, $h = 50\ and\ 150\ \mu m$ allows to cover the above cited shear rates range.

The flow rates Q_R and Q of the reference fluid and of the fluid to be characterized are precisely controlled using two accurate micro-syringe pumps. As a reference Newtonian fluid, an aqueous solution was used with a viscosity of $\eta_R = 6\ mPa \cdot s$ at $T = 25^oC$.

Due to the small size of the channel and the range of involved flow rates, the flows are laminar and fully developed at the channel outlet. The actual position of the interface occupied by the fluids is measured by acquiring a time series of images of the interface between the two fluids and thanks to a subsequent image processing. The ratio of the transverse extents of the two fluids W/W_R near the outlet of the micro-fluidic device is proportional to the ratio of the apparent viscosity η_{app} of the fluid to be characterized and the known viscosity η_R of the reference fluid,[7,8]:

$$\frac{W}{W_R} = \frac{\eta_{app}}{\eta_R}\frac{Q}{Q_R} \tag{1}$$

Thus, according to the simple relationship above, monitoring optically the ratio $\frac{W}{W_R}$ and knowing the flow rates Q and Q_R allows one to extract the ratio $\frac{\eta_{app}}{\eta_R}$ between the apparent viscosity of the fluid to be characterized to the known viscosity of the reference fluid.

The true rate of shear experienced by the fluid to be characterized may be expressed according to Weissenberg-Rabinowitsch-Mooney equation,[1]:

$$\dot{\gamma}_{true} = \frac{\dot{\gamma}_{app}}{3}\left[2 + \frac{d\ \ln\dot{\gamma}_{app}}{d\ \ln\tau}\right] \tag{2}$$

Here $\dot{\gamma}_{app} = \frac{6Q}{Wh}$, h is the height of the micro-channel,[9] and $\tau = \dot{\gamma}_{true}\eta = \dot{\gamma}_{app}\eta_{app}$ is the true stress imposed onto the tested fluid.

In closing this part we note that the principle of the operation of the micro-fluidic rheometer does not cover the study of yield stress fluids as it only provides viscosity upon shear stress.

Notes and references

1 C. W. Macosko, *Rheology: principles, measurements, and applications*, Wiley, New York, 1994.

2 P. Coussot, *Rheometry of pastes, suspensions and granular materials*, John Willey & Sons, 2005.

3 *year*.

4 E. N'gouamba, M. Essadik, J. Goyon, T. Oerther and P. Coussot, *Rheologica Acta*, 2021, **60**, 653–660.

5 J. Sepulveda, A. Montillet, D. D. Valle, T. Amiar, H. Ranchon, C. Loisel and A. Riaublanc, *Applied Rheology*, 2021, **31**, 24–38.

6 V. Carnicer, C. Alcàzar, M. Orts, E. Sánchez and R. Moreno, *Open Ceramics*, 2021, **5**, 100052.

7 P. Guillot, P. Panizza, J.-B. Salmon, M. Joanicot, A. Colin, C.-H. Bruneau and T. Colin, *Langmuir*, 2006, **22**, 6438–6445.

8 P. Nghe, E. Terriac, M. Schneider, Z. Z. Li, M. Cloitre, B. Abecassis and P. Tabeling, *Lab Chip*, 2011, **11**, 788–794.

9 C. Miller, *Industrial & Engineering Chemistry Fundamentals*, 1972, **11**, 524–528.